2020-1132 IJOI
https://www.ijoi-online.org/

International Journal of Organizational Innovation

A NEW SLOPE STABILITY ANALYSIS METHOD CONSIDERING THE TECTONIC EARTHQUAKE EFFECTS

Tse-Shan Hsu
President, Institute of Mitigation for Earthquake Shear Banding Disasters
Professor, Department of Civil Engineering, Feng-Chia University, Taiwan R.O.C.
tshsu@fcu.edu.tw

Lin-Yao Wang
Student, Ph.D. Program for Civil Engineering, Water Resources Engineering, and Infrastructure Planning, Feng-Chia University, Taiwan, R.O.C.

Chang-Chi Tsao, Hong-Chia Chang
Directors, Institute of Mitigation for Earthquake Shear Banding Disasters, Taiwan R.O.C.

Tsai-Fu Chuang
Associate Professor, Department of Civil Engineering, Feng-Chia University, Taiwan R.O.C.

Abstract

For ground vibrations occurring along with shear banding during tectonic earthquakes, the primary and secondary effects of tectonic earthquakes is shear banding and ground vibration, respectively. In previous slope stability analyses of large-scale landslide areas, the adopted slope stability analysis methods have all neglected the influence from the primary effect of tectonic earthquakes, and the obtained results do not match the actual requirements. To resolve upon this issue, a slope stability method considering shear banding and ground vibration effects is proposed. The large-scale landslide of Tsaoling in Taiwan from the Jiji earthquake is taken as an

example for an in-depth discussion on the influence of shear banding effect in slope stability analysis. As indicated by the results in the slope stability analysis for this large-scale landslide, when neglecting shear banding and vertical ground vibration effects, the resulting shear resistance strength parameters of the sliding surface from the back-calculation will be significantly lower. From the forward-calculation, the resulting factor of safety from slope stability analysis will also be significantly reduced. As found in the remediation of large-scale landslide areas, when significantly lower shear resistance strength parameters are adopted in the design, long-term stability in these remediated areas will not be maintainable. Therefore, it is recommended that when conducting slope stability analyses for large-scale landslide areas, either using back-calculation or forward-calculation, the proposed slope stability analysis method should be adopted.

Keywords: slope stability, tectonic earthquake, shear banding, ground vibration.

Introduction

Taiwan is situated at the edge of the Eurasian Plate, and is under the compression from the Philippine Sea Plate. From the epicenter distribution map of historical earthquakes shown in Figure 1, tectonic earthquakes in Taiwan are very frequent. As can be observed in the Global Positioning System (GPS) velocity vector distribution map of Taiwan shown in Figure 2, there are various velocity vectors in Taiwan with varying magnitude or direction.

As defined by Hsu (1987), when the velocity vectors are in the same direction yet have different magnitudes, a slip-type shear band exists in between the two adjacent points. Conversely, when the velocity vectors have the same magnitude with different directions, there is twinning-type shear band in between the two adjacent points. Therefore, from Figure 2, there is clear slip-type or twinning-type shear bands in various regions of Taiwan.

Considering the lateral compression of tectonic plates, Hsu (2018) simulated the formation of shear bands (see drawings of Step 1 in Figure 3 for details), and the corresponding ground vibrations during shear banding (see plots of Step 2b and Step 3 in Figure 3 for details).

Figure 1. Distribution of historical epicenters in Taiwan (1995-2016) (background image is taken from Google Earth, 2020; Earthquake Monitoring Report Center, Central Weather Bureau, MOTC, 2020).

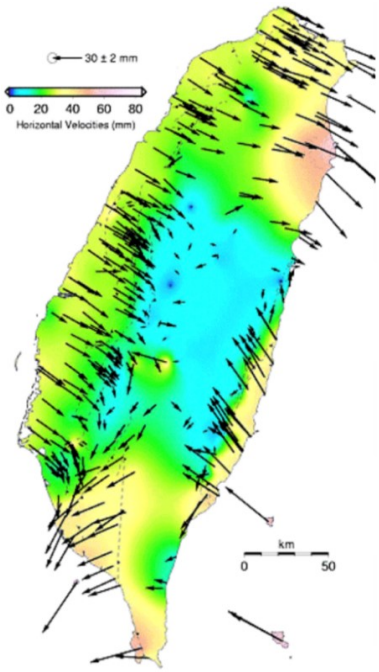

Figure 2. GPS velocity vector distribution in Taiwan (2007/1/1-2007/12/31) (GPS LAB, 2020)

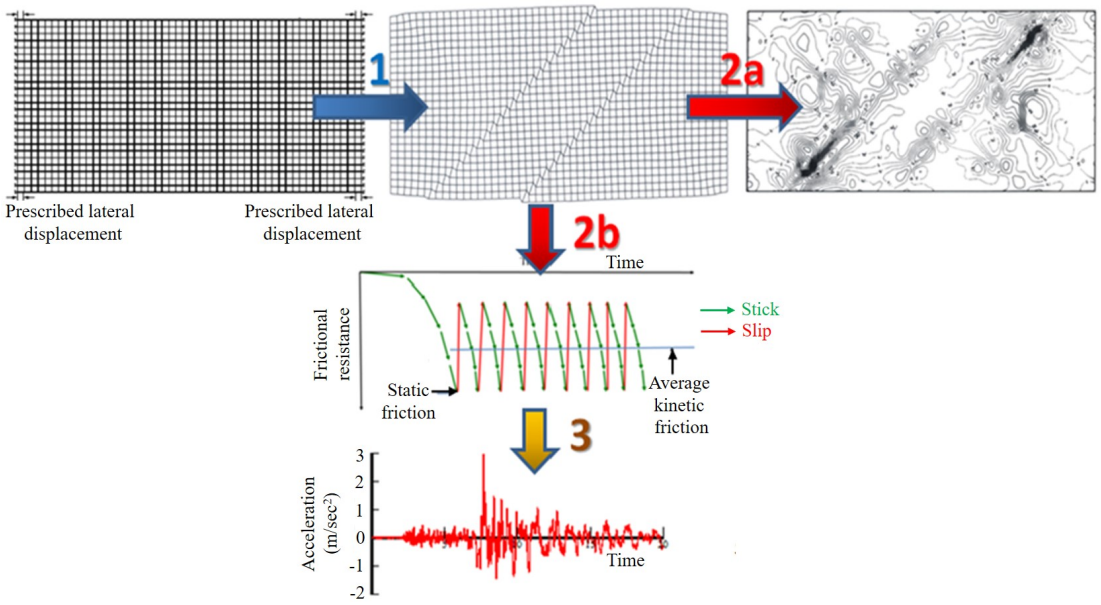

Figure 3. Process for the shear band formation under lateral compression of tectonic plates, as well as highly concentrated excess pore water pressure and ground vibration induced by shear banding (Hsu, 2018).

Step 1 in Figure 3 demonstrates that when the strain goes deep into plastic range, localizations of deformations of the tectonic plate will appear due to the loss of ellipticity caused by material strain softening, and further derive the shear bands (Drucker, 1950; Hill, 1962; Mandel, 1966; Rudnicki and Rice, 1975; Rice, 1976; Valanis, 1989) and the shear banding tilted slopes (Hsu, 2018). Step 2a presents the highly concentrated excess pore water pressure induced locally by shear banding. Step 2b shows the repeated stick-slip phenomenon induced by frictional resistance during the shear banding. Finally, Step 3 shows the ground vibrations induced by the repeatedly occurring stick-slip phenomenon.

The overwhelming majority of earthquakes are tectonic earthquakes, and the effects of tectonic earthquakes as shown in Figure 3 include shear banding and ground vibration. Shear banding is the primary effect (accounting for more than 90% of the total energy in tectonic earthquakes) and ground vibration is a secondary effect (only accounting for less than 10% of the total energy of tectonic earthquakes) (Coffey, 2019; Hsu, Tsao, and Lin, 2017).

Since the amount of shear banding will continuously accumulate from

all previous tectonic earthquakes and the amount of ground vibrations will vanish after an earthquake (Hsu, 2018), the degree of brittle fracture in rocks in shear bands of multi-step tilted slopes (see Figure 4 for details) will increase along with an increasing amount of shear banding, and large-scale sliding failure will occur during normal periods, heavy rain, or tectonic earthquakes.

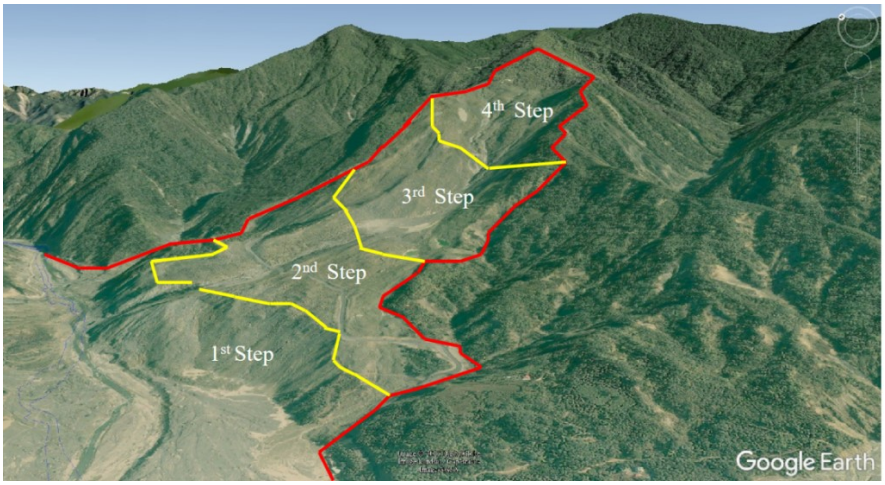

Figure 4. Large-scale landslide occurred in Xiaolin Village, Taiwan in 2009 (background image is taken from Google Earth, 2020).

As recorded by Chang and Lee (1989), Lee et al. (1993), Hung (1980), and Huang et al. (1983), the Tsaoling areas had three sliding failures in 1861, 1941, and 1979 before the 1999 Jiji earthquake. Furthermore, the use of satellite image mapping was uncommon until recently, and therefore, considering the lack of historical image mapping, it is difficult to evaluate the authenticity of changes in terrain in the Tsaoling landslide areas before and after the Jiji earthquake, as mentioned by Lee (2011) and Hung, et al. (2000) (see Figure 5 for details).

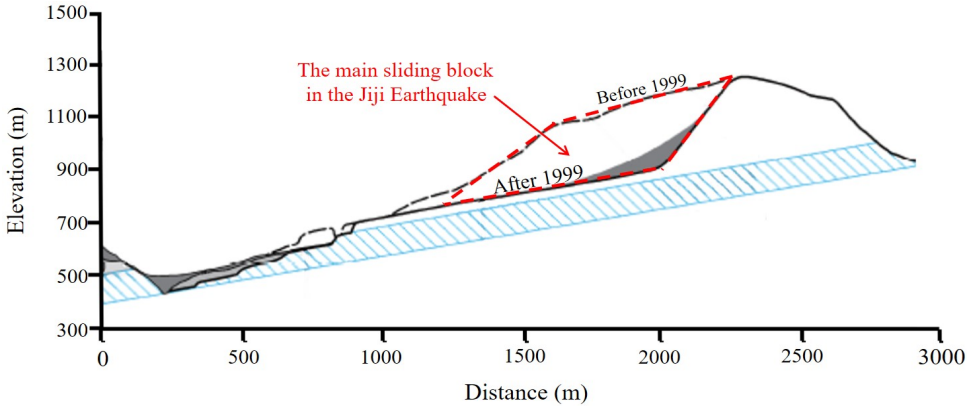

Figure 5. Terrain changes in the Tsaoling landslide area induced by the Jiji earthquake (redrawn from Lee, 2011).

By comparing the historical satellite images before and after the Jiji earthquake (see Figure 6(a) and Figure 6(b) for details), the change in the terrain of the Tsaoling landslide area from the Jiji earthquake can be evaluated. From Figure 5 and Figure 6 the following can be observed: (1) the total length of the Tsaoling landslide area is approximately 2324.5 m with an average thickness of approximately 24 m, with the sliding failure belonging to a type of delamination sliding failure; (2) the total length of the main sliding block in the Tsaoling landslide area drawn by Lee (2011) is approximately 780 m long with an average thickness of approximately 310 m; and (3) the main sliding block as drawn by Lee (2011) is not actually in the Tsaoling landslide area as shown in Figure 6. (4) As for the landslides in Tsaoling that occurred in 1941 and 1979, Hung, Lin, and Lee (2020) used a horizontal acceleration coefficient of $k_h = 0.18$ and factor of safety of $FS = 1.0$ solely considering the effect of horizontal ground motions, and back-calculated the shear resistance strength parameters of all sliding surfaces in all tilted slopes, finding an adhesion of $c_\alpha = 0$ kPa and a friction angle of $\delta = 20^o$.

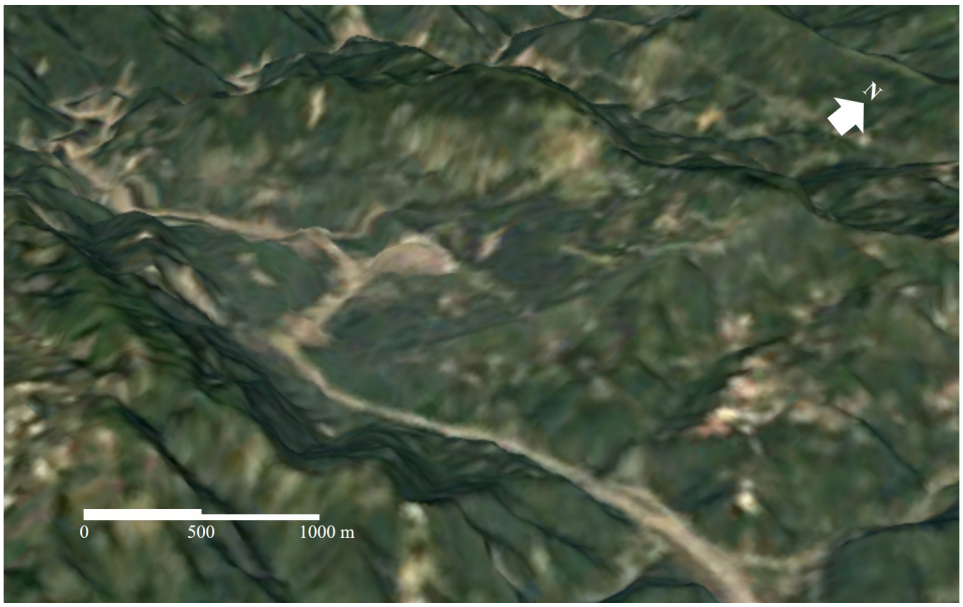

(a) Before the Jiji earthquake (December 1998)

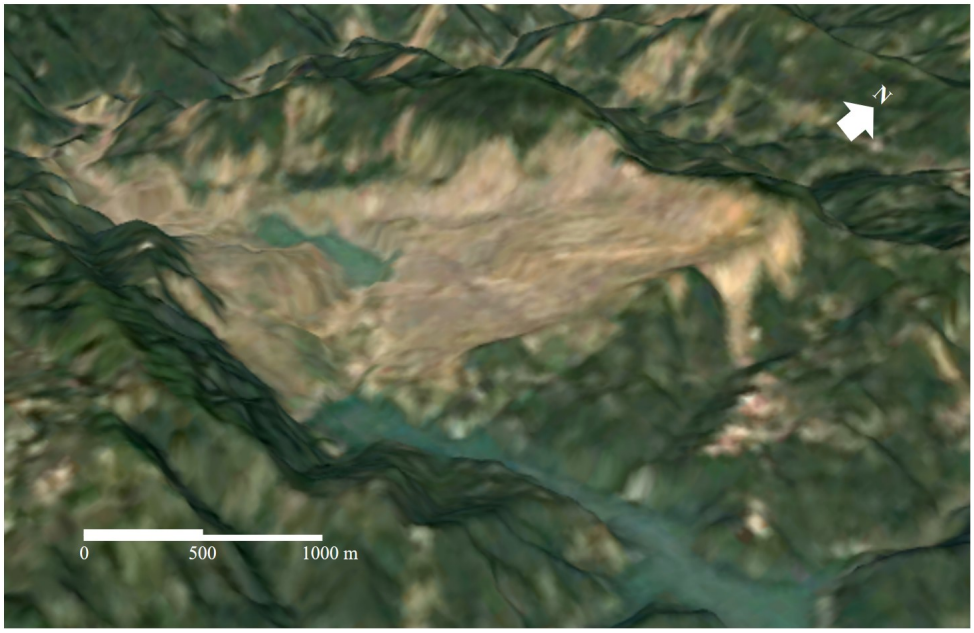

(b) After the Jiji earthquake (December 2000)

Figure 6. The satellite images before and after the Jiji earthquake in 1999 show the delamination sliding failure of the large landslide area in Tsaoling (Google Earth, 2020).

To align the slope stability analysis results for shear banding tilted slopes with actual needs, a new slope stability analysis method for shear banding tilted slopes is first developed, and the Tsaoling sliding failure from the Jiji earthquake is then taken as an example for the slope stability analysis. The results demonstrate that the slope stability analysis method for tectonic earthquakes needs to consider both shearing banding and horizontal and vertical ground vibration effects to obtain analysis results that meet actual requirements.

Proposed Slope Stability Analysis Method

Shear banding effect

Figure 7 shows a sliding block with dual sliding surfaces formed at the intersection of a gentle slope and a steep slope. When the formation of the steep slope is caused by the uplifting action of shear banding, Figure 7 shows that the shear textures within an overall shear band demonstrate principal displacement shear, thrust shear, Riedel shear, conjugate Riedel shear, and compression textures (Tchalenko, 1968). Therefore, the hanging wall shown in Figure 7 will continue to be lifted during the shear banding of tectonic earthquakes, whereas the foot wall remains relatively stationary.

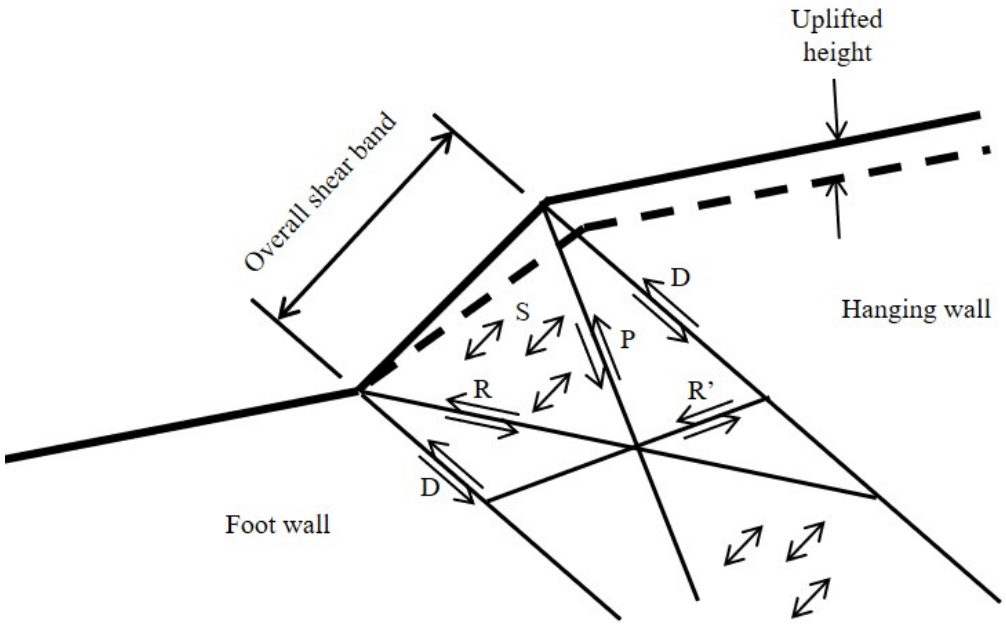

Figure 7. The shear banding that causes the hanging wall to continuously rise relative to the foot wall.

Slope stability analysis model

First, to address the shear banding and ground vibration effects in tectonic earthquakes, a new slope stability analysis model as shown in Figure 8 is proposed. In Figure 8, a shear banding force of P_s is acting on the top of the upper sliding surface and the direction of P_s is perpendicular to the upper sliding surface. The horizontal and vertical ground vibration forces acting on the upper sliding block are k_hW_1 and $-k_vW_1$, respectively, and the horizontal and vertical ground vibration forces acting on the lower sliding block are k_hW_2 and $-k_vW_2$, respectively.

As for the shear banding force P_s, it is assumed that both the right side of the upper sliding block and the left side of the lower sliding block have tension cracks due to shear banding, and the steeper upper sliding surface is caused by the uplifting effect of shear banding from tectonic earthquakes. Under these conditions, when the amount of shear banding continuously accumulates until the slope is on the verge of failure, the shear banding force P_s is approximately equal to half of the upper sliding block weight $W_1/2$.

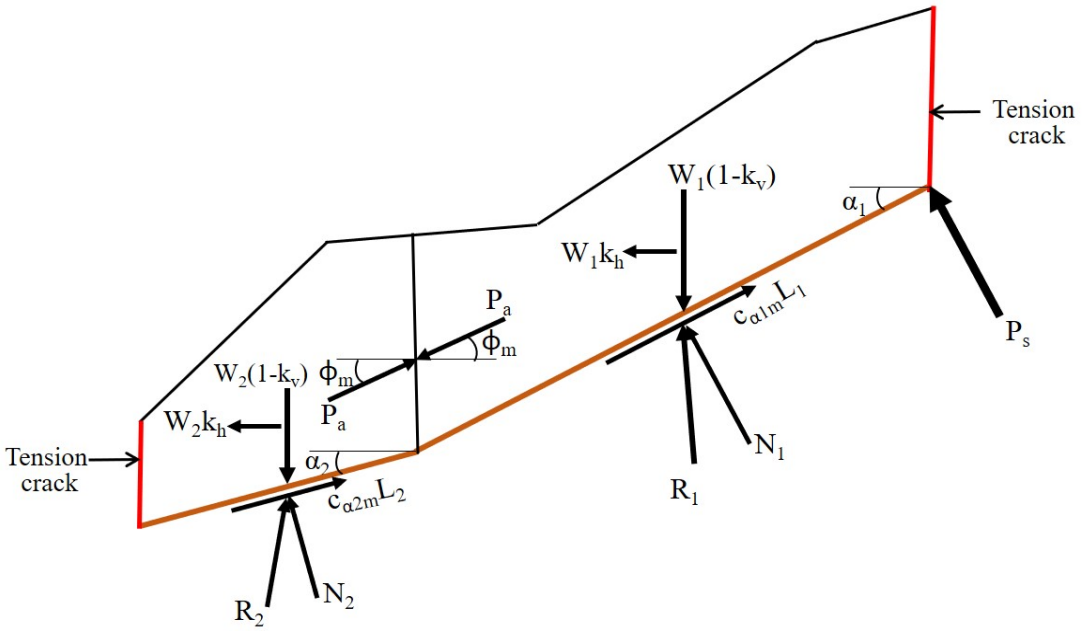

Figure 8. The proposed slope stability analysis model with dual sliding surfaces between two tension cracks.

Next, when a landslide in Tsaoling occurs, the groundwater level is lower than the sliding surface, and thus the slope stability analysis results would not be affected. Therefore, as shown in Figure 8, the required parameters or material properties for the slope stability analysis of the Tsaoling landslide area include: (1) the upper sliding block weight W_1, normal component of W_1 on the upper sliding surface N_1, length of the upper sliding surface L_1, inclination angle α_1, adhesion c_{a1}, friction angle δ_1, resultant force from the friction and adhesion resistances R_1, and shearing banding force P_s; and (2) lower sliding block weight W_2, normal component of W_2 on the lower sliding surface N_2, length of the lower sliding surface L_2, inclination angle α_2, adhesion c_{a2}, friction angle δ_2, and the resultant of the friction and adhesion resistances R_2.

As for the vertical interface between the upper and lower sliding blocks, under a static equilibrium, the active earth pressure of the upper sliding block P_{a1} and its angle of intersection with the horizontal plane φ_1 need to equal the active earth pressure of the lower sliding block P_{a2} and its angle of intersection with the horizontal plane φ_2, respectively; therefore, the factor of safety that satisfies the relationships of $P_{a1} = P_{a2} = P_a$ and $\varphi_1 = \varphi_2 = \varphi$ is the factor of safety FS desired in the analysis..

For the forces acting on the upper and lower sliding blocks as shown in Figure 8, under static equilibrium, Figure 9a and 9b present the closed force polygons of all forces acting on the upper sliding block and lower sliding blocks, respectively.

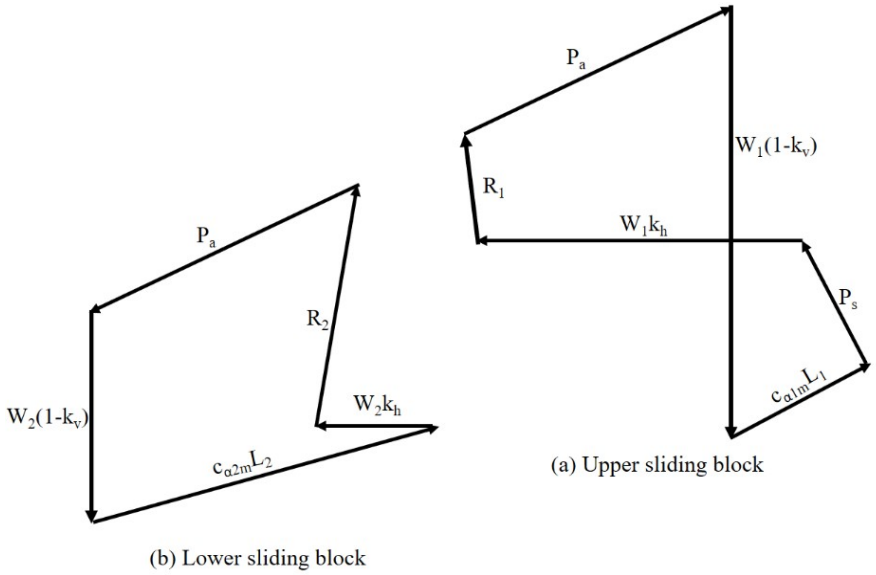

Figure 9. Force polygons for the upper and the lower sliding blocks.

For the upper sliding block, the closed force polygon shown in Figure 9a can be used as supplemented by the horizontal and vertical force balances, or $\sum F_h = 0$ and $\sum F_v = 0$. The active earth pressure for the upper sliding block P_{a1} is thus given in Equation 1 as

$$P_{a1} = A^* / [\cos\phi_m + \sin\phi_m \tan(\alpha_1 - \delta_{1m})] \quad \text{(Equation 1)}$$

where

$$A^* = [W_1(1-k_v) - P_s\cos\alpha_1 - c_{\alpha 1m}L_1\sin\alpha_1]\tan(\alpha_1 - \delta_{1m}) + W_1k_h + P_s\sin\alpha_1 - c_{\alpha 1m}L_1\cos\alpha_1$$

Next, for the lower sliding block, the closed force polygon shown in Figure 9b can be used as supplemented by horizontal and vertical force balances of $\sum F_h = 0$ and $\sum F_v = 0$, respectively. The active earth pressure of the lower sliding block P_{a2} is given by Equation 2 as

$$P_{a2} = B^* / [\cos\phi_m + \sin\phi_m \tan(\alpha_2 - \delta_{2m})] \quad \text{(Equation 2)}$$

where

$$B^* = -[W_2(1-k_v) - c_{\alpha 2m} L_2 \sin\alpha_2]\tan(\alpha_2 - \delta_{2m}) - W_2 k_h + c_{\alpha 2m} L_2 \cos\alpha_2$$

Numerical algorithm

Since the force balance conditions for the upper and lower sliding blocks needs to be met at the same time, a trial and error method can be used by first assuming a factor of safety of $FS_{assumed}$. Subsequently, Equation 1 can be used to calculate the active earth pressure acting on the upper sliding block P_{a1}, and then Equation 2 used to calculate the active earth pressure acting on the lower sliding block P_{a2}. Finally, after the calculated value of P_{a1}-P_{a2} is less than the error tolerance ε, $FS_{assumed}$ is then equal to the slope stability factor of safety *FS*.

Based on this trial and error method, a calculation procedure was written to obtain the slope stability factor of safety *FS* (see Table 1 for details).

Table 1. The calculation procedure for the factor of safety of the slope stability analysis.

(1) Let $FS_{assumed}$ = 0.001 and the error tolerance be ε = 0.001;
(2) Calculate $\phi_m = \phi / FS_{assumed}$, $\delta_{1m} = \delta_1 / FS_{assumed}$, $\delta_{2m} = \delta_2 / FS_{assumed}$, $c_{a1m} = c_{a1} / FS_{assumed}$, and $c_{a2m} = c_{a2} / FS_{assumed}$;
(3) Use Equation (1) and Equation (2) to calculate the active earth pressures P_{a1} and P_{a2}, respectively;
(4) Calculate the difference ΔP_a between P_{a1} and P_{a2};
(5) When ΔP_a is less than ε, the safety factor $FS = FS_{assumed}$, and stop the calculation after outputting FS;
(6) Otherwise, let $FS_{assumed} = FS_{assumed} + 0.001$, GO TO (2), and continue the calculation.

Case Analysis

In this study, the large-scale Tsaoling landslide induced by the 1999 Jiji earthquake was selected as a case study for the slope stability analysis.

Analysis conditions

Case 1: For the case considering both the shear banding effect and the horizontal and vertical ground vibration effects of tectonics earthquakes, the back- calculation for the slope stability analysis was conducted. I.e., for $FS = 1.0$, where the shear banding force of the upper sliding block is $P_s = W_1/0.5$, and the horizontal and vertical ground vibration acceleration coefficients are k_h and k_v, respectively. From the back-calculation, the shear resistance strength parameters such as the adhesion $c_{\alpha 1}$ and the friction angle δ_1 of the upper sliding surface, and the adhesion $c_{\alpha 2}$ and the friction angle δ_2 of the lower sliding surface were calculated.

Case 2: A back-calculation for the slope stability analysis was performed for the case considering the horizontal and vertical ground vibration effects. I.e., for $FS = 1.0$, where the horizontal and vertical ground vibration acceleration coefficients are k_h and k_v, respectively. From the back-calculation, the shear resistance strength parameters such as the adhesion $c_{\alpha 1}$ and the friction angle δ_1 of the upper sliding surface, and the adhesion $c_{\alpha 2}$ and the friction angle δ_2 of the lower sliding surface were calculated.

Case 3: Under the joint action of the shear banding and horizontal and vertical ground vibration force effects of tectonic earthquakes, the back-calculation results of Case 1 and Case 2, and the back-calculation results of Hung, Lin, and Lee (2020) were used to compute the slope stability factors of safety *FS* for the five sliding block steps.

Analysis data

1) From Figure 10, the total length of the sliding surface in the Tsaoling landslide area is 2324.5 m. Point A to K can be roughly divided into five shear banding tilted slope steps: ABC, CDE, EFG, GHI, and IJK.

2) Each step in the shear banding tilted slope has a relatively gentle slope segment, AB, CD, EF, GH, and IJ, and a relatively steep slope segment, BC, DE, FG, HI, and JK. Using the sliding failure mechanism of multi-step shear banding tilted slopes of Hsu (2018), it is found that after sliding failure of the first step, each of the following steps will have a sliding failure in succession.

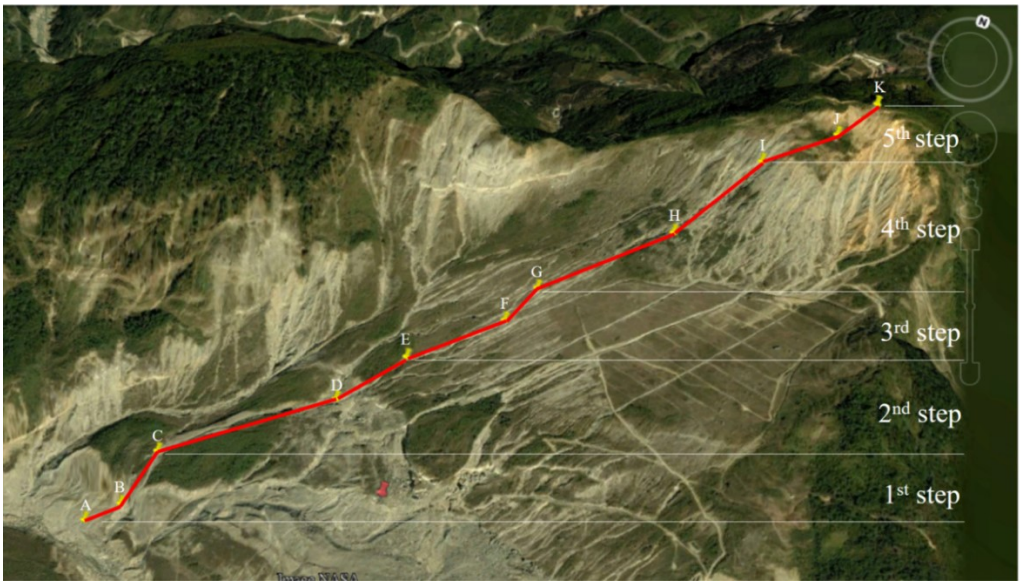

Figure 10. Five steps appeared in the Tsaoling sliding surface during the Jiji earthquake (background image is taken from Google Earth, 2020).

For the slope stability analysis of the Tsaoling landslide area, the coordinates for Point A to K, horizontal distance ΔX, elevation difference ΔY, and inclination angle of each line segment for Figure 10 are recorded in Table 2.

For the sliding surfaces of the five non-shear banding zones AB, CD, EF, GH, and IJ as shown in Figure 10, the unit weight for the corresponding sliding blocks is 24.52 kN/m^3, while those for the five shear banding zones BC, DE, FG, HI, and JK is 20.60 kN/m^3.

Table 3 presents the corresponding relationship between the PGA and seismic acceleration coefficients as provided by the Ministry of Economic Affairs (2008).

Table 2. The coordinates of each nodal point, ΔX, ΔY, and inclination angle of each line segment in the sliding planes shown in Figure 10.

Nodal Point	X-Coord (m)	Y-Coord (m)	Line Segment	ΔX (m)	ΔY (m)	Inclination Angle (degee)
A	0.00	0.00	AB	119.00	1.00	0.5
B	119.00	1.00	BC	111.89	141.00	51.6
C	230.88	142.00	CD	466.02	115.00	13.9
D	696.90	257.00	DE	198.31	66.00	18.4
E	895.21	323.00	EF	259.22	64.00	13.9
F	1154.43	387.00	FG	117.73	32.00	15.2
G	1272.15	419.00	GH	347.39	112.00	17.9
H	1619.55	531.00	HI	249.03	128.00	27.2
I	1868.58	659.00	IJ	200.95	61.00	16.9
J	2069.52	720.00	JK	121.27	57.00	25.2
K	2190.79	777.00	--	--	---	---

Table 3. Corresponding relationship between PGA and seismic acceleration coefficients (Ministry of Economic Affairs, 2008)

PGA	k_h
<0.12g	0.10
0.12g~0.18g	0.10~0.12
0.18g~0.50g	0.12~0.16
0.50g~0.80g	0.16~0.24
>0.80g	0.24
Note: $k_v = k_h \times R$, $R \geq 0.5$.	

From Table 3 and the distribution map of peak acceleration for the landslide area in Tsaoling as presented by Hsu (2002), the peak ground acceleration (PGA) for the five step sliding blocks in the Tsaoling landslide area can be obtained as shown in Table 4. Then, Table 3 can be used to obtain the

horizontal seismic acceleration coefficient k_h and vertical seismic acceleration coefficient k_v corresponding to each PGA (see Table 4 for details).

Table 4. The k_h and k_v corresponding to each PGA for the five step sliding blocks in the Tsaoling landslide area during the Jiji earthquake.

Sliding block	PGA (g)	k_h	k_v
1st step	0.5	0.16	0.08
2nd step	0.8	0.24	0.12
3rd step	>0.8	0.24	0.12
4th step	>0.8	0.24	0.12
5th step	>0.8	0.24	0.12

In the slope stability analysis for the five stepped shear banding tilted slopes, the shear banding forces P_s, the horizontal ground vibration forces of the upper sliding block, the vertical ground vibration forces of the upper sliding block, the horizontal ground vibration forces of the lower sliding block, and the vertical ground vibration forces of the lower sliding block are shown in Table 5.

Table 5. The shear banding forces and ground vibration forces used in the case study for the shear banding tilted slopes.

Shear banding tilted slopes	Shear banding forces	Ground vibration forces			
		Upper sliding block		Lower sliding block	
	P_s (kN)	W_1k_h (kN)	$-W_1k_v$ (kN)	W_2k_h (kN)	$-W_2k_v$ (kN)
1st Step: ABC	44485	14235	-7118	11204	-5601
2nd Step: CDE	51652	24793	-12396	67785	-33892
3rd Step: EFG	30151	14472	-7236	37706	-18853
4th Step: GHI	69198	33215	-16608	51546	-25773
5th Step: IJK	33116	15896	-7948	29656	-14828

Analysis result

Case 1: The shear resistance strength parameters obtained through back-calculation are shown in Table 6 for when the shear banding force and the horizontal and vertical ground vibration forces from tectonic earthquakes are all considered.

Table 6. Shear resistance strength parameters obtained through back-calculation under the condition that the shear banding effect and horizontal and vertical ground vibration forces are considered.

	Upper sliding plane		Lower sliding plane 2	
	Adhesion $c_{\alpha 1}$ (kPa)	Friction angle δ_1 (degree)	Adhesion $c_{\alpha 2}$ (kPa)	Friction angle δ_2 (degree)
1st Step: ABC	0	30.0	38.89	31.0
2nd Step: CDE	0	30.0	42.69	31.5
3rd Step: EFG	0	30.0	40.63	31.3
4th Step: GHI	0	32.0	123.36	36.0
5th Step: IJK	0	31.8	90.39	35.0

Case 2: Table 7 presents the shear resistance strength parameters obtained through back- calculation when only the horizontal and vertical ground vibration forces from tectonic earthquakes are considered.

Table 7. Shear resistance strength parameters obtained through back-calculation when only horizontal and vertical ground vibration forces are considered.

	Upper sliding plane		Lower sliding plane 2	
	Adhesion $c_{\alpha 1}$ (kPa)	Friction angle δ_1 (degree)	Adhesion $c_{\alpha 2}$ (kPa)	Friction angle δ_2 (degree)
1st Step: ABC	0	28.0	7.22	28.2
2nd Step: CDE	0	29.5	9.00	29.7
3rd Step: EFG	0	29.0	7.48	29.0
4th Step: GHI	0	32.0	51.89	34.0
5th Step: IJK	0	31.0	42.86	32.5

Case 3: Table 8 presents the slope stability analysis and factor of safety *FS* results for the back-calculations of Case 1, Case 2, and for the back-calculations of Hung, Lin and Lee (2020) under the joint action of the shear banding and horizontal and vertical ground vibration forces from tectonic earthquakes.

Table 8. Slope stability factor of safety *FS* as obtained through the analysis using the back-calculation results of Case 1, Case 2 and Hung, Lin and Lee (2020) under the joint action of shear banding and horizontal and vertical ground vibration forces.

Shear banding tilted slope	Using the back-calculation results of Case 1	Using the back-calculation results of Case 2	Using back-calculation results of Hung, Lin and Lee (2020)
	FS	FS	FS
1st Step: ABC	1.000 (100%)	0.578 (57.8%)	0.120 (12.0%)
2nd Step: CDE	1.000 (100%)	0.457 (45.7%)	0.134 (13.4%)
3rd Step: EFG	1.000 (100%)	0.473 (47.3%)	0.136 (13.6%)
4th Step: GHI	1.000 (100%)	0.575 (57.5%)	0.130 (13.0%)
5th Step: IJK	1.000 (100%)	0.566 (56.6%)	0.131 (13.1%)

Comparison And Discussion Of Analysis Results

1) Figure 11 shows the GPS velocity vector distribution map in the vicinity of the Tsaoling landslide area induced by the Jiji earthquake. From Figure 11, the velocity vectors between each two adjacent points appear to be different in magnitude or direction, thereby proving that there are shear bands of slip-type (blue line), conjugate slip-type (green line), twinning-type (yellow line), and conjugate twinning-type (red line) in the Tsaoling landslide area (see Figure 12).

2) From the amount of horizontal shear banding between each two adjacent points in the Tsaoling landslide area shown in Figure 12 as well as the inclination angle of sliding surface shown in Figure 10 and Table 2, the amount of uplifting for the hanging wall can be obtained.

3) Since the shear banding effect is the primary effect of tectonic earthquakes, the shear banding force P_s induced by the uplift of the hanging wall is the main driving force for the sliding failure of the shear banding tilted slope in tectonic earthquakes.

4) For slope stability analysis methods that only consider the secondary effects of tectonic earthquakes, the slope stability analysis results from neither back-calculations nor forward-calculations are consistent with the observed behavior.

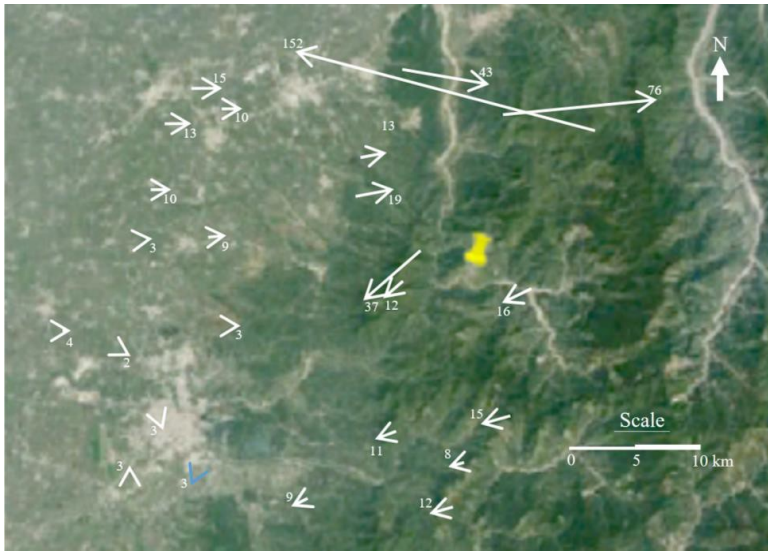

Note: The yellow needle point is the Tsaoling landslide area, and the unit is cm.

Figure 11. The GPS velocity vector distribution map in the vicinity of the Tsaoling landslide area induced by the Jiji earthquake (Google Earth, 2020; National Land Surveying and Mapping Center, 2002).

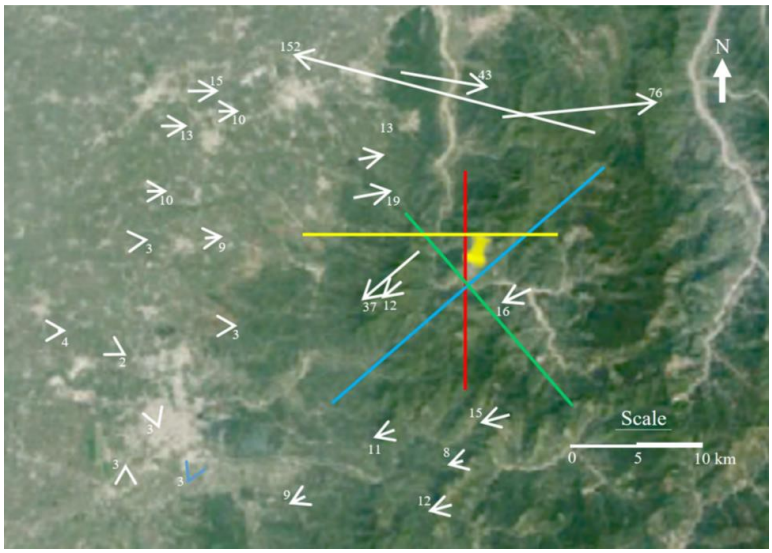

Note: The yellow needle point is the Tsaoling landslide area, and the unit is cm.

Figure 12. The shear bands existing in the vicinity of the Tsaoling landslide area identified by the GPS velocity vector distribution map (background image is taken from Google Earth, 2020 and National Land Surveying and Mapping Center, 2002).

5) Both the void ratio and water permeability of brittle fractured rock in shear banding zones are high. Rainwater after infiltration easily flows into the pore space of shear banding zones, washing out floating smaller diameter particles, thereby causing the change in gradation of brittle fractured shear banding rock debris. As a result, the potential sliding blocks gradually lose stability and the sliding velocity gradually quickens, thereby leading to sliding failure under the primary effects of tectonic earthquakes.

6) Since the large-scale landslides occur only in the shear banding zones, and the shear resistance of rock debris in the shear banding zones increases with increasing depth, the degree of brittle fracture decreases with increasing depth. Therefore, the depth of the sliding surface in the large-scale landslide area is mostly less than 25 m (see Hsu, Chen, and Lai, 2007).

7) As for the five step sliding blocks in the Tsaoling landslide area, under three different conditions that are "simultaneously considering shear banding and horizontal and vertical ground vibration effects", "consideration of only horizontal and vertical ground vibration effects", and "consideration of only horizontal ground vibration effects", the back-calculation results demonstrate the following:

(1) From the comparison of back-calculation results under the three different conditions as shown in Table 9: (a) for the upper sliding surface of each step sliding block located at the shear band, the adhesion $c_{\alpha 1}$ is equal to 0 kPa; (b) the friction angle δ_1 for the upper sliding surface on each sliding block shows back- calculation results that are "lower" or "severely lower" for "consideration of only horizontal and vertical ground vibration effects" or "consideration of only horizontal ground vibration effects", respectively; (c) when "only considering the horizontal and vertical ground vibration effects", the back- calculation results show that the maximum percentage lower than the actual required value of the friction angle δ_1 for upper sliding surface is 7%; (d) when "consideration of only horizontal ground vibration effect", the back- calculation results show that the

maximum percentage lower than the actual required value of friction angle δ_1 for the upper sliding surface is 37.5%.

Table 9. Comparison of back-calculation results under three different conditions (for upper sliding plane).

	Consider the influence of P_s, k_hW_1 and $-k_vW_1$		Only consider the influence of k_hW_1 and $-k_vW_1$		Only consider the influence of k_hW_1*	
	$c_{\alpha 1}$	δ_1	$c_{\alpha 1}$	δ_1	$c_{\alpha 1}$	δ_1
1st Step: ABC	0	30.0° (100%)	0	28.0° (93%)	0	20° (66.7%)
2nd Step: CDE	0	30.0° (100%)	0	29.5° (98.3%)	0	20° (66.7%)
3rd Step: EFG	0	30.0° (100%)	0	29.0° (96.7%)	0	20° (66.7%)
4th Step: GHI	0	32.0° (100%)	0	32.0° (100%)	0	20° (62.5%)
5th Step: IJK	0	31.8° (100%)	0	31.0° (97.5%)	0	20° (62.9%)

* : Back-calculation results provided by Hung, Lin and Lee (2020).

(2) From the comparison of back-calculation results under the three different conditions as shown in Table 10: (a) the cohesion $c_{\alpha 2}$ and friction angle δ_2 for the lower sliding surface as obtained through back-calculation demonstrate "lower" or "severely lower" results for "consideration of only horizontal and vertical ground vibration effects", or "consideration of only horizontal ground vibration effects", respectively; (b) for "consideration of only horizontal and vertical ground vibration effects", the maximum percentage lower than the actual required value of the adhesion $c_{\alpha 2}$ for the lower sliding surface as obtained through back-calculation is 81.6%, and the maximum percentage lower than the actual required value of the friction angle δ_2 is 9%; (c) For "consideration of only horizontal ground vibration effect", the maximum percentage lower than the actual required value of

the adhesion $c_{\alpha 2}$ for the lower sliding surface as obtained through back-calculation is 100%, and the maximum percentage lower than the actual required value of the friction angle δ_2 is 44.6%.

Table 10. Comparison of back-calculation results under three different conditions (for lower sliding plane).

	Consider the influence of P_s、k_hW_2 and $-k_vW_2$		Only consider the influence of k_hW_2 and $-k_vW_2$		Only consider the influence of k_hW_2	
	$c_{\alpha 2}$	δ_2	$c_{\alpha 2}$	δ_2	$c_{\alpha 2}$*	δ_2*
1st Step: ABC	38.89(100%)	31.0°(100%)	7.22(18.6%)	28.2°(91.0%)	0 (0%)	20°(64.5%)
2nd Step: CDE	42.69(100%)	31.5°(100%)	9.00(21.4%)	29.7°(94.3%)	0 (0%)	20°(63.5%)
3rd Step: EFG	40.63(100%)	31.3°(100%)	7.48(18.4%)	29.0°(92.7%)	0 (0%)	20°(63.9%)
4th Step: GHI	123.36(100%)	36.0°(100%)	51.89(42.1%)	34.0°(94.4%)	0 (0%)	20°(55.6%)
5th Step: IJK	90.39(100%)	35.0°(100%)	42.86(47.4%)	32.5°(92.9%)	0 (0%)	20°(57.1%)

*：Back-calculation results provided by Hung, Lin and Lee (2020).

8) For the scenario considering the shear banding effect and horizontal and vertical ground vibration effects of tectonic earthquakes, using the back-calculation results of three different conditions as "consideration of shear banding and horizontal and vertical ground vibration effects", "consideration of only horizontal and vertical ground vibrating effects", and "consideration of only horizontal ground vibration effect" for the slope stability analysis of the Tsaoling landslide area, the factors of safety *FS* obtained from the analysis are tabulated in Table 8. The calculation results of *FS* indicate the following:

(1) Under the actions of shear banding and horizontal and vertical ground vibration effects from tectonic earthquakes, when using the back-calculation results "considering only horizontal and vertical ground vi-

bration effects" for the slope stability analysis, the obtained factor of safety FS_b is only 45.7% to 57.8% of the actual required factor of safety FS_a.

(2) Under the actions of shear banding and horizontal and vertical ground vibration effects from tectonic earthquakes, when using the back-calculation results "considering only the horizontal ground vibration effect" (Hung, Lin, and Lee, 2020) for the slope stability analysis, the factor of safety obtained from the analysis FS_c is only 12.0% to 13.6% of the actual required factor of safety FS_a.

Conclusions And Suggestions

For large-scale landslide areas induced by tectonic earthquakes, all current slope stability analysis methods do not consider the primary effect of tectonic earthquakes (shear banding effect), thus preventing the analysis results from meeting actual requirements. Furthermore, many large-scale landslide areas in Taiwan often have a reoccurrence of sliding failure after remediation. To address this, the present study proposed a new slope stability analysis method that considers shear banding and ground vibration effects, and used the case study results of the Tsaoling landslide area to obtain the following three conclusions:

1) For large-scale landslides induced by tectonic earthquakes, satellite imagery shows that such landslides include multi-step shear banding tilted slopes. Due to the action of the shear banding, slope stability analyses for such landslide areas should be conducted separately with a focus on the shear banding tilted slope of each step, so that the results obtained can meet actual requirements.

2) When the slope stability analysis is conducted for large-scale landslides induced by tectonic earthquakes, to obtain accurate back-calculated shear resistance strength parameters, the sliding failure mechanism adopted in the analysis will need to be match the actual sliding failure mechanism in tectonic earthquakes, and the forces adopted in the analysis must be in accordance with those present during tectonic earthquakes.

3) As shown by the results from the case study on the large-scale Tsaoling landslide area:

(1) For the upper sliding surfaces in

the shear banding zones, when only the effects of the horizontal and vertical ground vibration effects were considered, the maximum percentage lower than the actual required value for the back calculated friction angle was 7%; when only the effect of the horizontal ground vibration effect was considered, the maximum percentage lower than the actual required value for the back calculated friction angle was 37.5%.

(2) For the lower sliding surfaces in the non-shear banding zones, when only the effects of the horizontal and vertical ground vibration effects were considered, the maximum percentages lower than the actual required values for the back calculated adhesion and friction angle were 81.6% and 9% respectively; when only the effect of the horizontal ground vibration effect was considered, the maximum percentages lower than the actual required values for the back calculated adhesion and friction angle were 100% and 44.4% respectively.

(3) When only the effects of the horizontal and vertical ground vibration effects were considered and the back calculated results were used for slope stability analyses, the maximum percentages lower than the actual required value for the calculated factor of safety was 54.3%; when only the effect of the horizontal ground vibration effect was considered and the back calculated results were used for slope stability analyses, the maximum percentage lower than the actual required value for the calculated factor of safety was 88.0%.

(4) For large-scale landslides resulting from tectonic earthquakes, the results of the case study show that either through back- or forward-calculation, only when both the shear banding effect (i.e. the primary effect) and ground vibration effects (i.e. secondary effects) of tectonic earthquakes are considered, can the slope stability analysis results accurately represent actual conditions.

Based on these three conclusions, the following two recommendations are made:

1) For large-scale landslide areas that have undergone sliding failure multiple times after remediation and within their life cycle during tectonic earthquakes, previous researchers have found that the sliding failure was due to excessive ground vibrations. However, based on the conclusions of this study, it is found that the cause of such sliding failure was that previous analysts only considered ground vibration effects (secondary effects), which are less than 10% of the total energy of tectonic earthquakes, when performing the required slope stability analysis, neglecting the shear banding effect (primary effect), which is more than 90% of the total energy. Therefore, it is recommended that the shear banding effect be included in the slope stability analysis method and future design codes.

2) For remediation projects of large-scale landslide areas maintain stability within their life cycle, it is recommended that the Design Code of Highway Slope Engineering (Ministry of Transportation and Communications, R.O.C.) be expanded according to the required consideration of the shear banding and ground vibration effects of tectonic earthquakes, thus enabling the proposed projects and methods to meet the design requirements for the primary and secondary effects of tectonic earthquakes at the survey, test, analysis, and design stages. Through this, remediation projects can meet the designed seismic performance for tectonic earthquakes.

References

Central Geological Survey of the Ministry of Economic Affairs, Integrated Geological Data Search System, website: Http://gis.moeacgs.gov.tw/gwh/gsb9 7-1/sys8/index.cfm, 2019.

Chang, S. Y., and Lee, C. T., “Geology and Collapse of Tsaoling area,” *Sinotech Engineering*, Vol. 19, pp. 27-43, 1989.

Coffey, J., “What are the Different Types of Earthquakes?” Universe Today, Space and astronomy news, Website: https://www.universetoday.com/82164/types-of-earthquakes/, 2019.

Drucker, D. C., “Some implications of work hardening and ideal plasticity,” *Quarterly of Applied Mathematics,* Vol. 7, No. 4, pp.

411-418, 1950.

Earthquake Monitoring Report Center, Central Weather Bureau, MOTC, Website: https://scweb.cwb.gov.tw/, 2020.

Google Earth, Website: http://www.google.com.tw/intl/zh-TW/earth/, 2020.

GPS LAB, Website: http://gps.earth.sinica.edu.tw/, 2020.

Hill, R., "Acceleration waves in solids," *Journal of the Mechanics and Physics of Solids,* Vol. 10, pp. 1-6, 1962.

Hsu, Tse-Shan, *Capturing Localizations in Geotechnical Failures*, Ph. D. Dissertation, Civil Engineering in the School of Advanced Studies of Illinois of Technology, 1987.

Hsu, T. S., "Distribution Map of Horizontal Peak Acceleration in Tsaoling Large-scale Landslide Area During the Jiji Earthquake," Department of Civil Engineering, Feng-Chia University, 2002.

Hsu, T. S., *The Major Cause of Earthquake Disasters: Shear Banding*, Institute of Mitigation for Earthquake Shear Banding Disasters, pp. 372-375, 2018.

Hsu, T. S., Chen, Chen, C. S., and Lai, S. Y., " Study on the Cracking Depth and Slippage of the Slope in the Catchment Area Caused by Strong Ground Vibration," *Journal of Hydraulic Engineering,* Vol. 17, PP. 210~226, 2007.

Hung, J. J., "A study on Tsaoling Rockslides," Taiwan, *Journal of Engineering Environment*, Vol. 1, pp. 29-39, 1980.

Hung, J. J., Lee, C. T., Lin, M. L., Lin, M. L., Jeng, F. S. and Chen, C. H., "A flying mountain and dam-up lake: Tsaoling rockslides," *Sino-Geotechenics*, Vol. 77, pp. 5-18. 2000.

Huang, J. S, He, H. C., Liu, H. J., "Geology and Landslides in Tsaoling Area in Central Taiwan," *Bulletin of the Central Geological Survey*, *MOEA*, Vo. 2, pp. 95-111, 1983.

Hung, J. J., Lin, M. L., Lee, C. T., "Analysis and Research on the Stability of Tsaoling Landslide Area," Website: http://gis.geo.ncu.edu.tw/GIS/slope/tsa

oling.htm. 2020.

Lee, C. T., "Geomorphological Evolution and Geology of the Tsaoling Rockslide," *Journal of Chinese Soil and Water Conservation*, Vol. 42, No. 4, pp. 325-335, 2011.

Lee, C. T., Hung, J. J., Lin, M. L. and Tsai, L. Y., *Engineering Geological Investigations and Stability Assessments on Tsaoling landslide Area*, A Specia1 Report Prepared for Sinotech Engineering Consultants, Inc., 1993.

Mandel, J., "Conditions de Stabilite et Postulat de Drucker," In *Rheologie et Mechanique des Sols* (Edited by J. Kravtchenko and P. M. Sirieys), Springer, 1966.

Ministry of Economic Affairs, R.O.C., "Derivation of Seismic Coefficient," *Technical Directions for Hydraulic Structures Inspection and Safety Evaluation, Reservoir and Water-Conveying Structures*, 2008.

Ministry of Transportation and Communications, R.O.C., *Design Code of Highway Slope Engineering*, Website: https://www.motc.gov.tw/en/index.jsp, 2015.

National Land Surveying and Mapping Center, Ministry of Internal Affairs, R.O.C., Taiwan, 921 Jiji Earthquake Survey Records, 2002.

Rice, J. R., "The Localization of Plastic Deformation," in Theoretical and Applied Mechanics (Proceedings of the 14th International Congress on Theoretical and Applied Mechanics, Delft, 1976, ed. W.T. Koiter), NorthHolland, Amsterdam, Vol. 1, pp. 207-220, 1976.

Rudnicki, J. W. and Rice, J. R., "Conditions for the localization of deformation in pressure-sensitive dilatants materials," *Journal of the Mechanics and Physics of Solids,* Vol. 23, pp. 371-394, 1975.

Tchalenko, J. S., "The evolution of kink-bands and the development of compression textures in sheared clays", *Tectonophysics*, Volume 6, pp. 159-174, 1968.

Valanis, K. C., "Banding and stability in plastic materials," *Acta Mech.* Vol. 79, pp. 113-141, 1989.